COMPLEX AIRCRAFT FUSELAGE FRAME MANUFACTURING USING AUTOMATED BRAIDING AND INFUSION

Monnot, P.[1,2,3], Levesque, J[2,3]. Dubé, R. [2,4], Laberge Lebel, L[1,2]*

[1] Advanced Composite and Fiber Structure laboratory (ACFSlab), Polytechnique Montréal, Mechanical Engineering Department, Montréal, Canada
[2] Research Center for High Performance Polymer and Composite Systems (CREPEC), Polytechnique Montréal, Montréal, Canada
[3] Groupe CTT, Saint-Hyacinthe, Canada
[4] Centre Technologique en Aérospatiale (CTA), Cégep Édouard-Montpetit, Saint-Hubert, Canada

*** Corresponding author (LLL@polymtl.ca)**

Keywords: *Textile Composites, Braiding, Infusion*

ABSTRACT

Automated manufacturing of carbon preforms for composite structures has shown to improve control and repeatability of the fiber orientation as well as to increase process speed. The high control on the reinforcement architecture combined to a low-cost resin infusion manufacturing offers cost saving potential for aircraft primary structure manufacturing. In this study, a complex mandrel was created for overbraiding. The mandrel has an arcuate shape. The rectangular cross-section has a constant width and a variable height along the mandrel. This variable cross-section reproduces typical fuselage frame geometrical variations (i.e. juggles) to accommodate fuselage skin features. This mandrel was mounted on an industrial manipulator and overbraided by guiding it through a 144-carrier radial braiding machine. The mandrel path and speed through the braiding machine is computed to achieve a well-defined braid microstructure. Three layers were braided to a target braid angle of 45° to enhance shear properties of the C-frame web. Axial fibers were inserted on the flanges to enhance the flexural stiffness of the C-Frame. The preform was subsequently infused with epoxy resin using 3D-printed caul surfaces. After curing, the part is cut in two halves and demolded from the mandrel to obtain two mirror-like C-frames. The parts were characterized using thickness measurements and microscopy to assess the high quality of the composite microstructure.

1 INTRODUCTION

Aircraft fuselage hoop frames are primary structures whose main functions are to support skin-stringer panels and to distribute concentrated loads [1]. The cross-section, typically a C, J or I section, varies to accommodate for skin thickness variations, pad-ups and joggles. As shown in Figure 1a, cuts-outs located the frame’s web and lower flange (mouse-holes or lightning hole) allow stringer and aircraft systems to pass through. Braided structural composites are potential replacements to traditional laminated composites made from prepregs cured in autoclave [2]. Combining a precisely controlled preform architecture to a low-cost resin infusion process provides a cost-effective material system to manufacture aircraft primary structures. Braided preforms are impregnated, cured, demolded and cut in half to obtain two mirror parts (Figure 1b). Braided frames were the subject of several recent R&D projects conducted by major aerospace companies such as Boeing [3], Airbus [4] and Bombardier [5]. Braided frames were even certified on the Boeing 787 program [6], which confirms this technology's potential (Figure 1c).

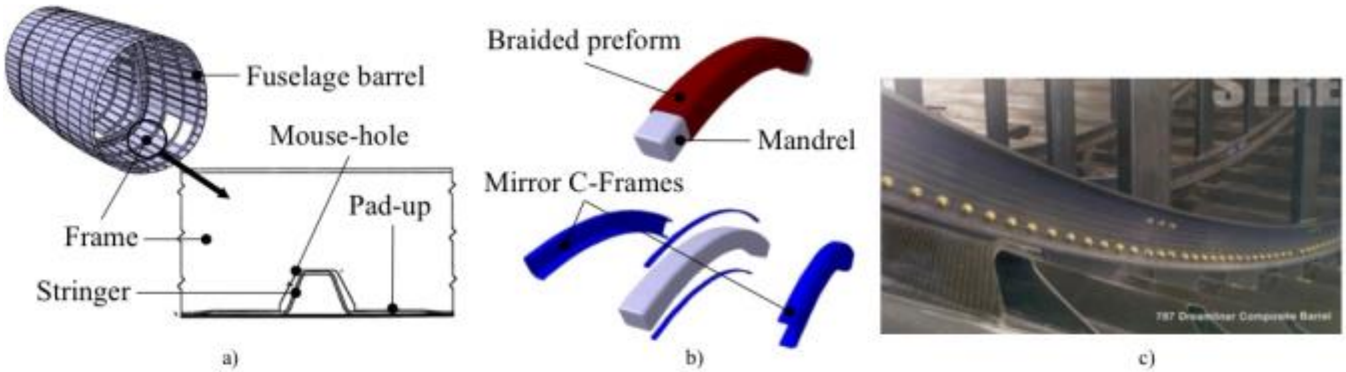

Figure 1. a) Fuselage frame configuration; b) Braided composites C-Frames manufacturing process [5]; c) Boeing 787 braided composites frames (From A&P).

Two-dimensional braiding is a traditional textile manufacturing process that produces braided preform, also referred as braids, used to manufacture braided structural composites. For most engineering applications, tubular braids are manufactured by overbraiding a mandrel through a radial or axial braiding machine as shown in Figure 2a [7]. Carbon fibre yarns are wound on spools and installed on the braiding machine's carriers. The number of carriers is specific to the braiding machine's design. Varying the number spools and their pattern modifies the preform's architecture. Thus, different braid patterns can be obtained, e.g. the regular braid (2/2) or the diamond braid (1/1) [8]. Biaxial braided preforms are manufactured by setting only bias carriers (i.e. weft and warp) with spools. Triaxial braided preforms can also be manufactured by intertwining longitudinal yarns along the mandrel's length. To do so, the braiding machine must be equipped with fixed external yarn carriers. Braided preforms are shaped from weft and warp yarns rotating in opposite directions. As shown in Figure 2a, Yarns converge through the guiding ring and then deposit onto the mandrel's surface at fell points. The highly interlaced architecture of braided preforms provides excellent damage tolerance properties [9]. It also conforms well to complex geometries, which provides near or near-net shape manufacturing (Figure 2b).

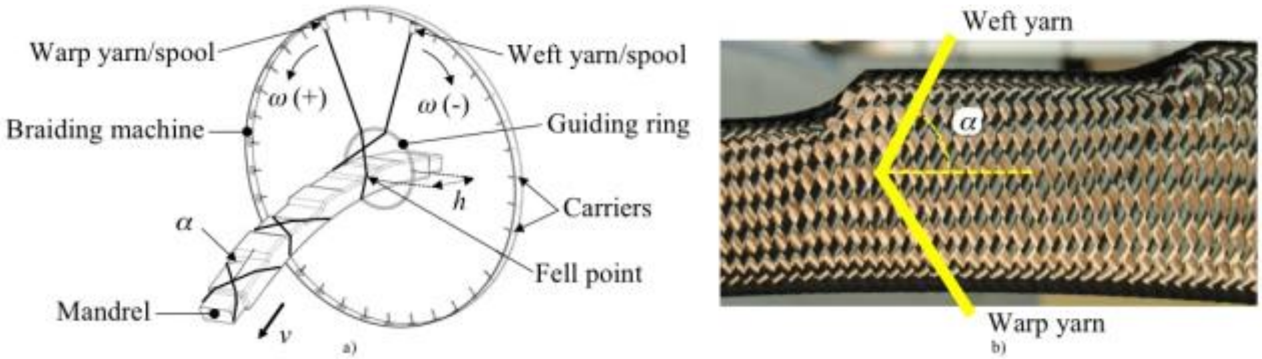

Figure 2. a) Braiding process representation; b) Braided preform over a complex mandrel.

Post-preforming operations, such as trimming or machining, can then be minimized, hence providing a cost saving potential [9]. The braiding process can be automated by installing the mandrel on a linear gantry or an industrial robot. Monnot *et al.* [10] exposed the benefits of automation on the process repeatability and productivity as well as the preforms quality. The mechanical performance of braided composites is mainly driven by the preform's architecture, namely the braid angle (α), fiber volume fraction (v_f) and thickness (t). These parameters are also critical for the fibre bed impregnation process since they directly influence the preform's permeability [9, 11]. Therefore, braiding models were developed to determine the required process parameters, the mandrel take-up speed (v) and the carriers rotational speed (ω) (Figure 2a), to be able to manufacture a specific preform architecture.

Dry braided preforms must be impregnated by the matrix polymer to create the composite component. Infusion is a low-cost process where the preform is secured between a one-sided mold and a membrane under vacuum. The resin is infused into the preform by means of a pressure differential. However, load-bearing composite structure manufacturing requires processes with thickness control. Accurate thickness control is usually achieved by using a costly two-sided molding process such as Resin Transfer Molding (RTM). To reduce tooling costs, we propose an innovative variation of the infusion process. Tailored caul surfaces matching the final part dimensions are built by 3D printing. These caul plates are integrated into the infusion process to ensure part dimensional consistency on the membrane side. Therefore, the objective of this study is to demonstrate the manufacturing feasibility of a complex fuselage C-Frame using braided composites and Structural Infusion$_{\text{TM}}$. The followed methodology and relevant results will be presented in the following sections.

2 EXPERIMENTAL

Two infusion scenarios were be conducted during experimentation. For the first experiment, a typical infusion process was used, where only vacuum pressure is applied to the bagged assembly. For the second experiment, once the preform is completely impregnated under vacuum pressure, the bagged assembly is placed into autoclave in order to provide an additional consolidation pressure during curing. The same braided preform architecture was used for both experiments.

2.1 Mandrel design

As previously stated, a C-Section was selected for the fuselage frame cross-section design. Typical design features present in an aircraft fuselage, namely mouse holes, pad-ups and joggles, were integrated to the mandrel's design. To do so, the height of the C-Section's web was varied along the mandrel's centerline. Both the length of the top and the bottom flanges were kept constant. In order to manufacture such a part, a non-dissolvable mandrel with a rectangular cross-section was manufactured. It's geometry and dimensions are presented in Figure 3a. REN shape 450 (Huntsman) was selected as the mandrel's material due its excellent machinability, dimensional and thermal stability. The mandrel's centerline has a constant radius of curvature, which is based on a typical medium-size business jet. Two mirror C-frames are obtained by cutting the cured composites in half. Grooves located on the top flange and the bottom flange were integrated to ease the cutting process. As shown in Figure 3b, the mandrel's functional length was divided into 17 sections, 9 constant and 8 varying, which excludes both end recesses. Yarn slipping occurs initially on the mandrel's surface when braiding over a non-axisymmetric cross-section. Both recesses act as "tampon" zones before the braid reaches the mandrel's functional length. They also help stabilize the braid during reverse braiding when a multiply preform is manufactured.

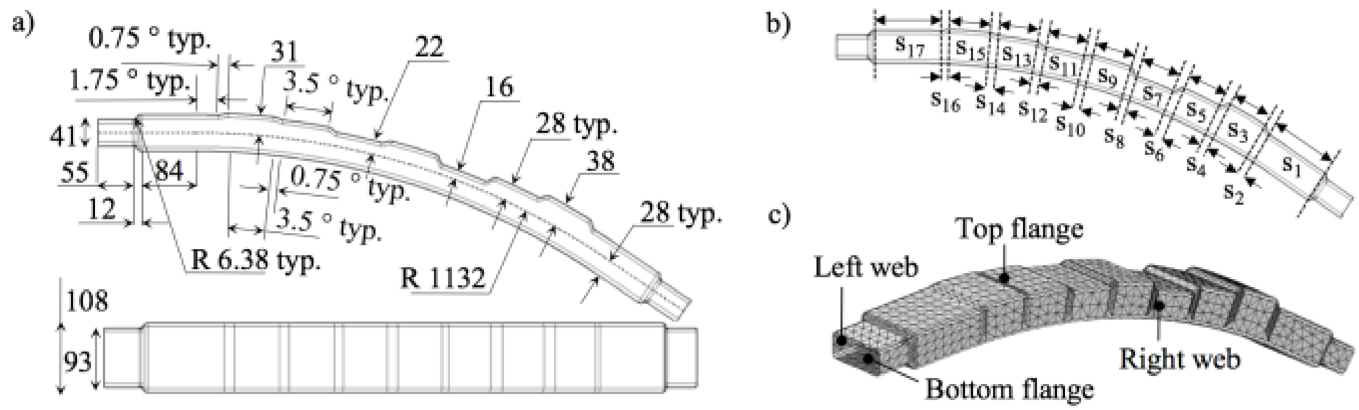

Figure 3. a) Mandrel shape and overall dimensions (in mm); b) Mandrel sections definition and numbering; c) Mandrel mesh and master faces.

2.2 2D braiding

2.2.1 Targeted preform architecture

The braided preform architecture was chosen to obtain the highest fiber volume fraction possible as well as following the aerospace industry typical design, a quasi-isotropic laminate. The target braid angle (α_t), i.e the angle between the weft and warp yarns in regards to the mandrel's centerline, was set to 45 °. This braid angle is ideal for the web since it reacts shear stress transferred from skin-stringer panels [1]. As for the flanges, they react tension and compression loads [1]. Therefore, axial yarns were added only on the flange faces in order to provide extra stiffness. The preforms were manufactured using a *Herzog* radial braiding machine which was equipped with a total of 144 bias carriers and 72 axial carriers. Spools were wound with *Tansome* carbon fiber tows (H2550 A10 12K/800 Tex). 36 spools per yarn group were installed on bias carriers and 13 spools per flange were installed on axial carriers. This spool pattern yields a diamond braid architecture (1/1) which provides the braided preform a maximum stability and firmness with minimum yarn slippage. Since the target braid angle is well under the braid jamming angle, interactions between yarns are minimized as well as crimp [12, 13]. However, a complete coverage of the mandrel is not ensured, especially on the web faces where less yarns are present. Therefore, three identical layers were braided on the mandrel's surface.

2.2.2 Non-circular braiding model

Braiding models are composed of an inverse and a forward solution. The inverse solution is used to determine the process parameters, the mandrel take-up speed (v) and the carriers rotational speed (ω), that are required to manufacture a specific preform architecture having a target braid angle (α_t). The forward solution provides the expected preform architecture, the expected braid angle (α_e), for a given set of process parameters. A novel cinematic non-circular braiding model, based the Van Ravenhorst *et al.* model [14], was developed for the complex C-Frame [15]. The mandrel take-up speed profile is determined from the yarns trajectories of the target preform architecture. As opposed to a circular cross-section mandrel, the mandrel take-up speed computed from the inverse solution varies with the mandrel's face. Therefore, the mandrel's surface was segmented into master faces to compute a mandrel take-up speed profile only based on specific faces. For this study, both web faces were selected as master faces since the cross-section variations are only achieved by varying their heights. Thus, the mandrel take-up speed profile follows the mandrel's geometrical variations adequately.

2.2.3 Process automation

The braiding process was automated with an industrial manipulator (*KUKA* KR100-HA) mounted on a linear axis. Presented in Figure 4, this 7 DOF robotic system allows a more accurate control on the mandrel's speed and motion than with a conventional gantry. It also provides the process a greater flexibility since mandrels with curved centerlines can be braided. During braiding, the manipulator moves the mandrel through the braiding machine's guiding ring. The mandrel is linked to the manipulators gripper with a connecting shaft. The required mandrel take-up speed profile is provided by the braiding model and the manipulator's trajectory is based on the mandrel's centerline. A multi-objective optimization algorithm based joint limits and singularity avoidance was developed by Monnot *et al.* [10] to plan the robot's motion along the desired trajectory. For each point of the trajectory, the robot's optimal positioning is determined, namely the joints angular positions and the robot's position on the linear axis. Prior to testing, the computed path planning is validated through visual simulation, then scripted and sent to the robot's controller.

Figure 4. Automated braiding system composed of a Herzog radial braiding machine and a KUKA industrial manipulator.

2.2.4 Preform characterization

The first of the two identical braided preforms was characterized once manufacturing was completed. An automated image acquisition process was developed to measure the braid angles over all four faces of the mandrel. To do so, the mandrel was moved by the manipulator under a fixed camera. One braid angle was measured numerically for each constant sections of the mandrel.

2.3 Structural Infusion$_{TM}$

The Structural Infusion$_{TM}$ main steps are presented at Figure 5. Before braiding, the mandrel was cleaned and treated with a sealer (Zyvax MPP 1006W, ChemTrend) and parting agent (Zyvax Waterworks Departure, ChemTrend). After braiding, 3D-printed (Firebird, SphereCo) nylon (ePA Nylon 6, eSun) caul surfaces were installed onto the preform (see Figure 5b) to help conform the preform to the mandrel. The caul surfaces dimensions were selected to achieve a target fiber volume content of 50%. The following bagging procedure is followed. A coated nylon peel-ply (Econolease, Airtech) is placed between the vacuum membrane and the caul surfaces. Resin feed line was placed onto the bottom flange between the two coal plates. Vacuum line was placed on the top flange. The assembly was covered by a vacuum tight membrane and submitted to a leak check. The room temperature curing resin (820 Marine / 824 hardener, Axson) resin was mixed and degassed during around 30 minutes. The resin was then transferred into the preform from the bottom flange to the top flange. When the preform was filled with resin, the resin valve was shut off and the setup stayed under vacuum for 24 hours for curing. For the second molding, the polymerisation was done within an autoclave (Econoclave 17B400C-2S2P6T, ASC Process Systems) (see Figure 5d) to benefit from a higher environmental gauge pressure of 2 bar. After curing, the part was trimmed and demolded to obtain two mirror C-frames. Part thickness was measured on equally spaced location at every section using a micrometer. One C-frame from the each of the two experiments was cut in pieces to extract cross-section microscopy coupons. The coupons were embedded in polyester (Technovit 4000, Anamet) and polished according to standard procedure. Images were acquired using a microscope (VHX-2000, Kenyence).

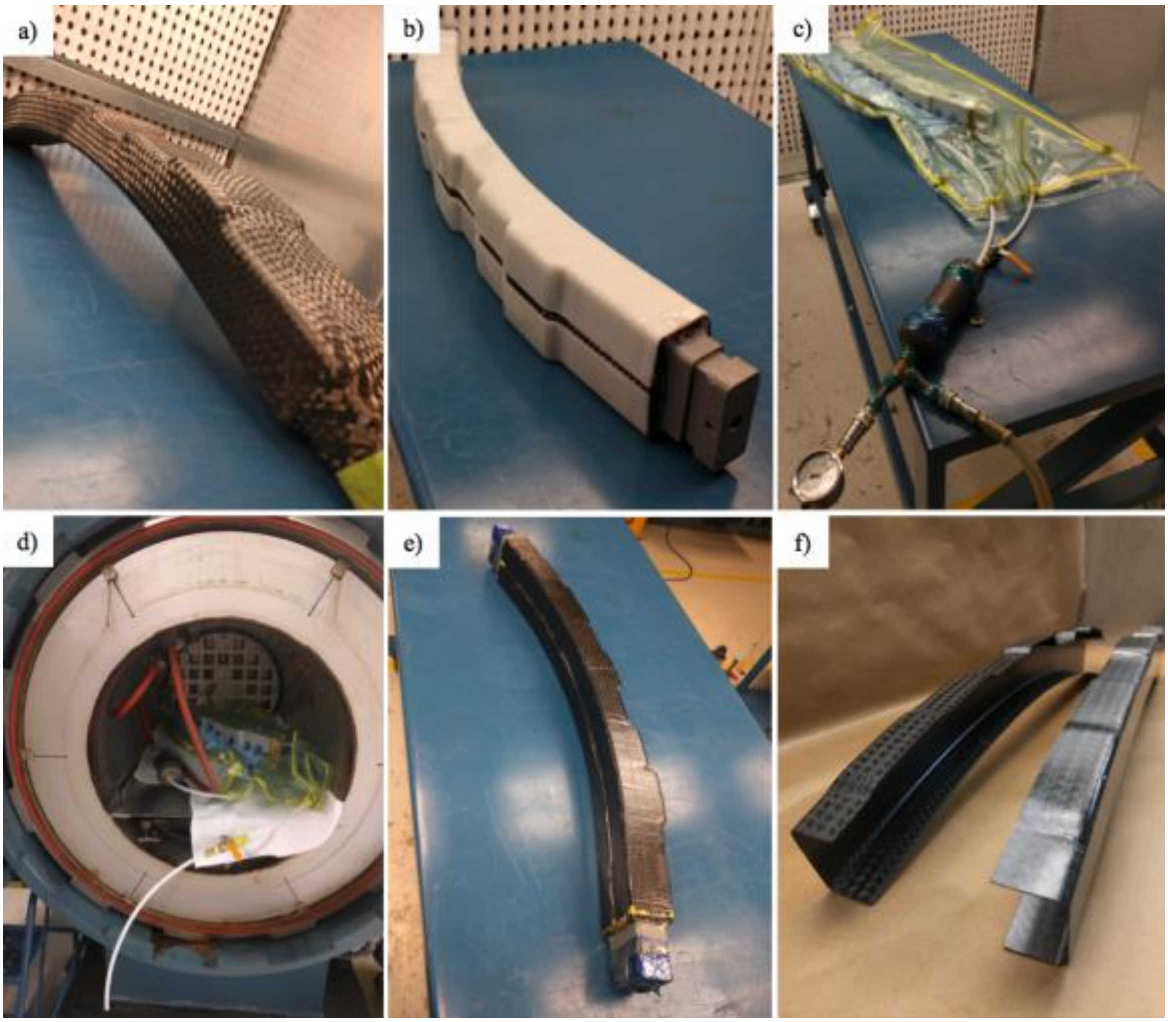

Figure 5. Structural Infusion$_{TM}$ Process: a) Braided preform on mandrel; b) Installation of 3D printed tailored caul surfaces; c) Bagging operation insuring appropriate vacuum level in composite and efficient resin distribution; d) After resin infusion, the part can be consolidated in an autoclave (optional); e) Consolidated and cured preform after debagging; f) Final trimmed components.

3 RESULTS AND DISCUSSION

3.1 Braiding

The target (α_t), expected (α_e), and measured (α_m) braid angle for the flange faces and the web faces for each constant sections of the mandrel are presented in Table 1.

Sections	Target braid angle (α_t)		Average expected braid angle (α_e)		Average measured braid angle (α_m)	
	Flanges (°)	Webs (°)	Flanges (°)	Webs (°)	Flanges (°)	Webs (°)
S3	45.0	45.0	47.2	48.5	53.0	50.0
S5	45.0	45.0	48.1	48.2	50.5	46.5
S7	45.0	45.0	48.2	44.3	50.0	46.0
S9	45.0	45.0	48.4	46.2	50.5	47.5
S11	45.0	45.0	48.9	48.6	50.5	47.0
S13	45.0	45.0	48.4	44.7	52.5	48.0
S15	45.0	45.0	48.9	44.3	52.5	50.0

Table 1. Target braid angle (α_t), average expected braid angle (α_e) and average measured braid angle (α_m) for the flange faces and the web faces for each constant sections of the mandrel.

As discussed earlier, the face length difference between the flanges and the webs causes a distribution of the braid angle over the mandrel's circumference. As shown in Table 1, the measured braid angle on the web faces is always smaller than on the flange faces. Using both webs as master faces to compute the mandrel take-up speed profile was beneficial as the measured braid angle on the web faces is closer to the target angle. The expected braid angle results are less conclusive. As shown in Table 1, some flange expected braid angles are higher than the web expected braid angle. A low number of yarns (35%) could deposit on the mandrel's surface when simulating deposition with the forward solution. Hence, causing discrepancies in the expected braid angle reported in Table 1. This phenomenon was caused by the mandrel take-up speed profile which wasn't well adapted to the mandrel's geometrical variations. Consequences of were also observed during physical overbraiding. As depicted in Figure 6, where braid bridging and yarn slipping occur over the sharpest cross-section transitions.

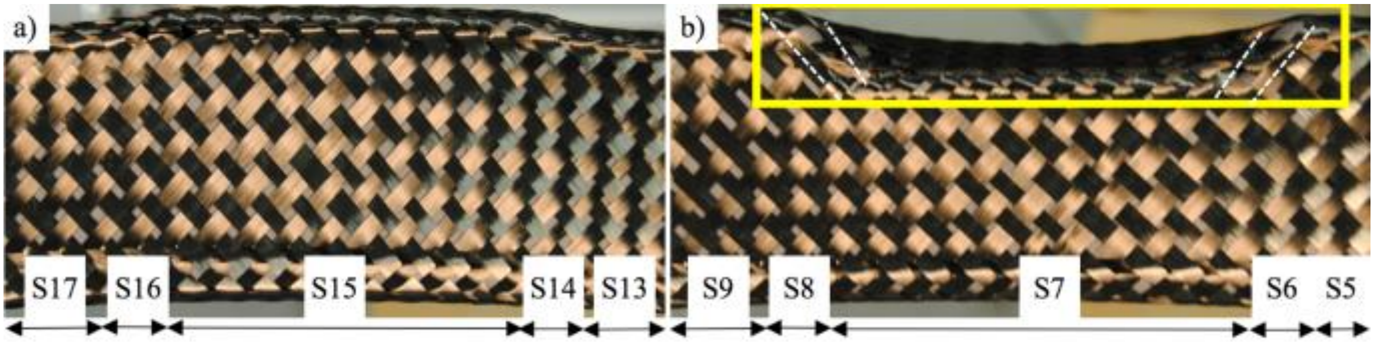

Figure 6. Braiding results: a) Constant braid architecture on transitions between section S13 and S17; b) Braid bridging on section S7 due to sharp transitions at S6 and S8. Yarn slipping on section S6 and S8 due to sharp transition.

3.2 C-Frame Infusion

Figure 7 shows selected cross-section micrographs from the autoclave-cured infused C-Frames. In general, micrograph inspection showed low void content. Figure 7a presents the radius from the web to the flange and indicates a good fiber distribution. Whiter yarn cross-sections are the axial yarns located mostly on the flange part of the cross-section. This is a confirmation that the automated braiding process can selectively reinforce the flange with axial yarns. Figure 7b) and c) are micrographs taken along the length of the top flange. It is seen that the fibre distribution and part thickness are uniform.

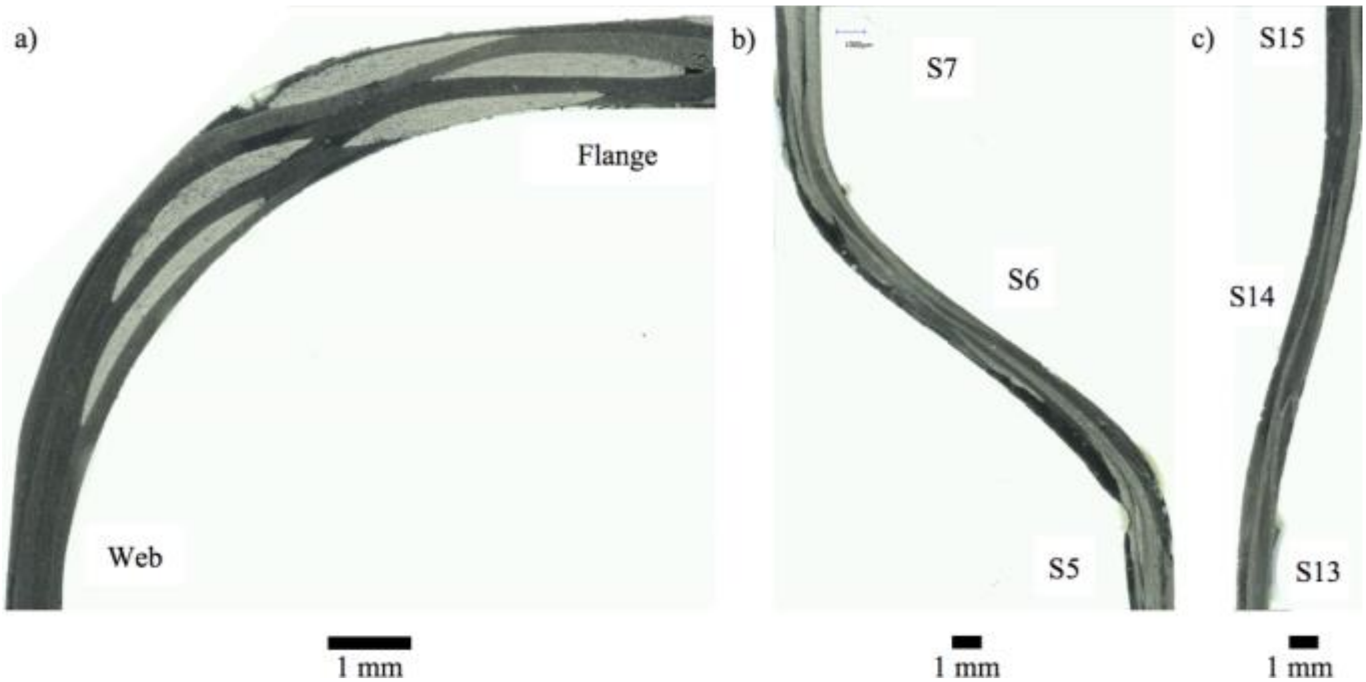

Figure 7. Selected micrographs taken on the autoclave-cured infused component: a) Radius between web and flange; b) Top flange with from section S5 to S7; c) Top flange from section S13 to S15.

Figure 8 shows the design and measured thicknesses for the atmospheric and autoclave-cured C-frames. It is seen that the atmospheric pressure cured C-frames could not consolidate to the design thickness for most of the top flange, bottom flange and web sections. The deviation is extreme on the top flange for all the steep cross-section changes from Section S3 to S8, where braid bridging was observed (see Figure 6b). The autoclave-cured C-frames' measured thicknesses are within the design values when considering the standard deviation. This indicates that for the braided preform tested, the atmospheric pressure could not apply a sufficient consolidation action to conform the braid onto the mandrel. A higher consolidation pressure applied in the autoclave could solve this issue.

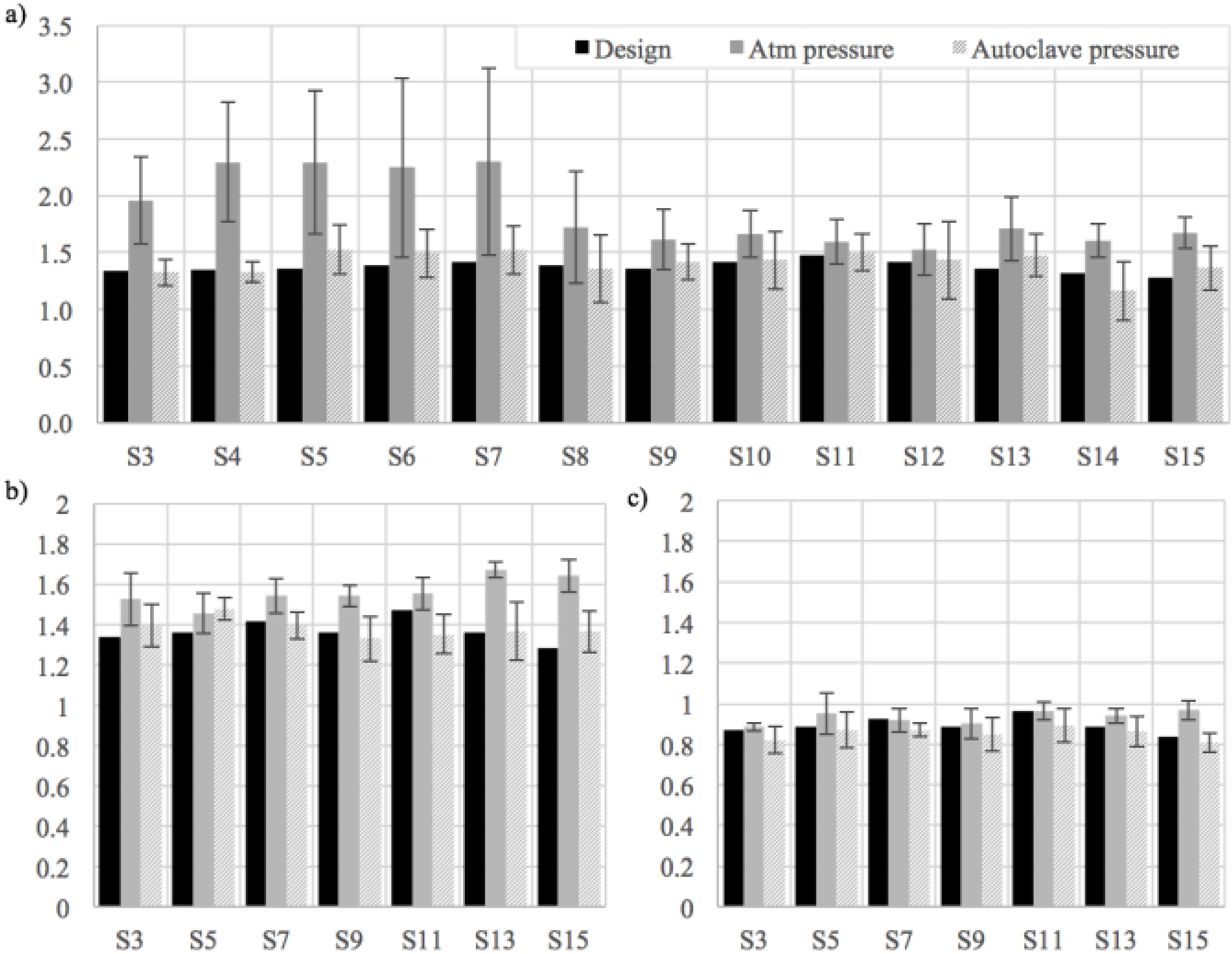

Figure 8. Frame thickness design values and measurements for the atmospheric and autoclave pressure cured parts: a) Top flange; b) Bottom flange; c) Web. Errorbars are standard deviations calculated on 18 measurements for top flange constant sections (uneven section numbers on a)). All other errorbars are standard deviations calculated on 6 measurements.

4 CONCLUSION

This study demonstrated the feasibility of the Structural Infusion$_{TM}$ of braided fuselage frames. It was seen that the automated braiding process could not produce a braid following the mandrel geometry for the selected braiding conditions. The consolidation pressure was not high enough during infusion and atmospheric pressure curing to consolidate the braid to the designed thickness. However, when applying a higher consolidation pressure during curing with the use of an autoclave, the final part thickness complies to the design requirements. This preliminary study opens many future research pathways. First, braid modelling and experimentation should be done to assess the global limitations in terms of mandrel cross-section changes. A preform thickness prediction tool should also be developed to ease caul surfaces design. Tooling materials should be screened and evaluated in detail to insure process performance and dimensional stability, especially for high temperature epoxy resins. With comprehensive understanding of all process parameters, it is envisioned that the Structural Infusion$_{TM}$ of braided preforms could serve as a low-cost manufacturing technique for aerospace fuselage frames.

5 ACKNOWLEGEMENTS

The authors wish to acknowledge the financial support from CREPEC (Integrator project grants) and the Natural Sciences and Engineering Research Council (NSERC, RGPIN-2016-06410) of Canada. The authors would also like to thank Alexandre Chagnon and Houda Boutkhil for their technical support

6 REFERENCES

1. Niu, C. and M.C.Y. Niu, *Airframe Structural Design: Practical Design Information and Data on Aircraft Structures*. 1999: Adaso Adastra Engineering Center.
2. Hoa, S.V., *Principles of the manufacturing of composite materials*. 2009: DEStech Publications, Inc.
3. Fedro, M.J. and K. Willden, 1992. "Characterization and manufacture of braided composites for large commercial aircraft structures."
4. Bulat, M., H. Ahlborn, F. Gnädinger, and D. Michaelis, *15 - Braided carbon fiber composites A2 - Kyosev, Yordan*, in *Advances in Braiding Technology*. 2016, Woodhead Publishing. p. 383-394.
5. Laberge Lebel, L. and P. Trudeau, 2013. "Preforming of a Fuselage C-Shaped Frame Manufactured by Resin Transfer Molding," SAE International Journal of Aerospace, **6**(2):508-512.
6. Kehrl, D.J. *Aerospace braided composite preform certification*. in *CAMX - The Composites and Advanced Materials Expo*. 2014. Orlando, FL.
7. Ko, F.K., 1987. "Braiding," ASM International, Engineered Materials Handbook., **1**:519-528.
8. van Ravenhorst, J.H. and R. Akkerman, *A spool pattern tool for circular braiding*, in *18th International Conference on Composite Materials, ICCM 2011*. 2011: Jeju Island, Korea.
9. Gutowski, T., *Advanced composites manufacturing*. 1997: John Wiley & Sons.
10. Monnot, P., L. J., O. Vermeersch, and L. Laberge Lebel, *Automated braiding of dry preforms for aerospace structural components*, in *SAMPE Long Beach 2016 Conference and Exhibition*. 2016: Long Beach.
11. Ko, F. and C. Pastore, 1988. "CIM of braided preforms for composites (Computer-Integrated Manufacturing)," Computer aided design in composite material technology:133-155.
12. Gao, Y.T., F.K. Ko, and H. Hu, 2013. "Integrated design for manufacturing of braided preforms for advanced composites part I: 2D braiding," Applied Composite Materials, **20**(6):1007-1023.
13. Michaeli, W., U. Rosenbaum, and M. Jehrke, 1990. "Processing strategy for braiding of complex-shaped parts based on a mathematical process description," Composites Manufacturing, **1**(4):243-251.
14. van Ravenhorst, J.H. and R. Akkerman, 2014. "Circular braiding take-up speed generation using inverse kinematics," Composites Part A: Applied Science and Manufacturing, **64**:147-158.
15. Monnot, P., J. Levesque, and L. Laberge Lebel, 2017. "Automated braiding of a complex aircraft fuselage frame using a non-circular braiding model," Composites Part A: Applied Science and Manufacturing, Submitted Manuscript No. JCOMA-17-595.